

WIND LOADS ON TRANSMISSION LINE STRUCTURES IN SIMULATED DOWNBURSTS

M.T. Chay ^a, F. Albermani ^a and H. Hawes ^b

^a *Department of Civil Engineering, University of Queensland, St Lucia QLD 4072 Australia*

^b *Powerlink Queensland, 33 Harold Street, Virginia, QLD 4014 Australia*

Downbursts pose a recognized threat to transmission line networks in South-east Queensland, and many other regions around the world. However, when assessing the structural adequacy of transmission line structures, design codes assume that an atmospheric boundary layer profile provide the basis of wind loading in the design process. Such assumptions may be leaving transmission networks exposed to an unquantified level of threat to a meteorological event that will likely cause the most severe loading on the structure during its lifetime.

An analytical/stochastic method of simulating downburst winds has been used to explore the quasi-static loading conditions that occur during downbursts. These are presented in comparison to several existing transmission tower design codes, and the implications with regard to the structural adequacy of transmission line structures is discussed

1. INTRODUCTION

The design of lattice structures such as transmission towers is recognised as a niche facet of structural engineering. As such, many countries have design codes that deal specifically with such structures. These include:

- AS3995-1994 (Australia)
- BS8100:Part 1:1986 (Britain)
- ANSI/TIA/EIA-222-F-1996 (USA)

Additionally, ESAA C(b) 1–2003 (Australia) describes requirements for overhead distribution and transmission networks. This document largely references AS/NZS 1170.2-2002 (the Australian wind loading code for general structures) for wind loading, although described conditions which are unique to electrical distribution and omitted in other Australian standards. All of these documents address the subject of wind loading as can be applied to lattice transmission structures.

Although there are degrees of variation between the design codes, one of the aspects which is common to all is the use of an atmospheric boundary layer profile to determine the design wind loading to be applied in the design process. With the exception of Sections A2.2 and A2.3 in ESAA C(b)1-2003, the wind loads produced during thunderstorms are largely left unaddressed.

Two types of wind events occur during thunderstorms that are of particular threat to transmission line structures. These are downbursts and tornadoes. In South East Queensland, and in many other parts of the world, downbursts are the dominant cause of severe wind gusts. This paper utilises an analytical/stochastic model of a downburst to examine the quasi-static wind loading conditions as they relate to lattice transmission line structures, and compares these loads to the codified boundary layer loads. However, the manner in which the various properties of a design wind are addressed varies slightly between the codes, making it difficult to directly compare each characteristic. As such, comparison in this paper will mostly focus on the differences between the Australian design codes, with a comparison of design loads on a theoretical tower presented at the end.

2. MODELS OF WIND

2.1 Boundary Layer Mean Speed.

The format of the boundary layer profile described in AS3995-1994 is the same as that in AS/NZS 1170.2-2002 (Australian Standard for Wind Loading on Structures), which is described by the Deaves and Harris model (AS/NZS 1170.2 Supp 1:2002) by the equation for the hourly mean speed profile shape as:

$$V_{m,z} = \frac{u^*}{0.4} \left[\log_e \left(\frac{z}{z_o} \right) + 5.75 \left(\frac{z}{z_g} \right) - 1.88 \left(\frac{z}{z_g} \right)^2 - \left(\frac{z}{z_g} \right)^3 + 0.25 \left(\frac{z}{z_g} \right)^4 \right] \quad (1)$$

Where $V_{m,z}$ is the hourly mean speed at height z , u^* is the friction velocity, z_0 is the roughness height, and z_g is the gradient height. For low heights, this is often abbreviated as

$$V_{m,z} = \frac{u^*}{0.4} \log_e \left(\frac{z}{z_0} \right) \quad (2)$$

Alternatively, there is a tabulated form of this data provided. Similarly, ESAA C(b)1-2003 directs users to AS1170.2-2002.

2.2 Downburst Wind Speed Model

From a structural engineering perspective, one of the most obvious differences between boundary layer and downburst winds is the shape of distribution of wind speed with a function of height. The downburst winds generally reach a peak somewhere between 50m and 100m AGL (Hjelmfelt 1988). The boundary layer winds, on the other hand, show a continuing non-linear increase in intensity until the gradient height has been reached. Further, unlike boundary layer winds, the so-called “mean”, or non-turbulent, wind speed in a downburst is a function of location in the horizontal plane with respect to the storm and varies with time, as well as being dependent on height. The distribution is also influenced by the translational speed of the storm.

In this paper, a parametric analytical method of simulating the non-turbulent winds of the downbursts is used. The radial (with respect to the centre of the storm) and vertical components of the wind are given by:

$$\bar{U}_r = 1.55 * \bar{U}_{r,max} \left(\frac{z}{5z_r} \right)^{1/6} \left[1 - \text{erf} \left(0.70 \frac{z}{5z_r} \right) \right] \frac{r}{r_i} e^{-\left[\frac{1-(r^2/r_i^2)^\alpha}{2\alpha} \right]} + \bar{U}_{Trans} \quad (3)$$

$$\bar{U}_z(x,y,z,t) = -2\Pi \frac{\bar{U}_{r,max} z_m}{r_p} \frac{\left\{ \frac{1}{c_1} [e^{c_1(z/z_r)} - 1] - \frac{1}{c_2} [e^{c_2(z/z_r)} - 1] \right\}}{[e^{c_1} - e^{c_2}]} \left[1 - \frac{1}{2} \left(\frac{r^2}{r_i^2} \right)^\alpha \right] e^{-\left[\frac{1-(r^2/r_i^2)^\alpha}{2\alpha} \right]} \quad (4)$$

where \bar{U}_r is the horizontal non-turbulent velocity, \bar{U}_z is the vertical non-turbulent velocity, Π is the intensity factor, α , c_1 , and c_2 are model constants (equal to 2, -0.15 and -3.2175 respectively), r is the radius to the point of observation in the horizontal plane from the centre of the storm ($r = (x^2 + y^2)^{0.5}$), z is the elevation above ground level to the point of observation, r_i is the time dependent radius to maximum velocity, z_m is the height of maximum wind speed at r_i , z_r is the height to maximum wind speed at r , erf is the error function, r_p is the radius to maximum wind speed corresponding to $\Pi=1$, $\bar{U}_{r,max}$ is the desired maximum radial speed from the downburst diverging winds, and \bar{U}_{Trans} is the storm translation speed.

Comparison of analytical model to full-scale data

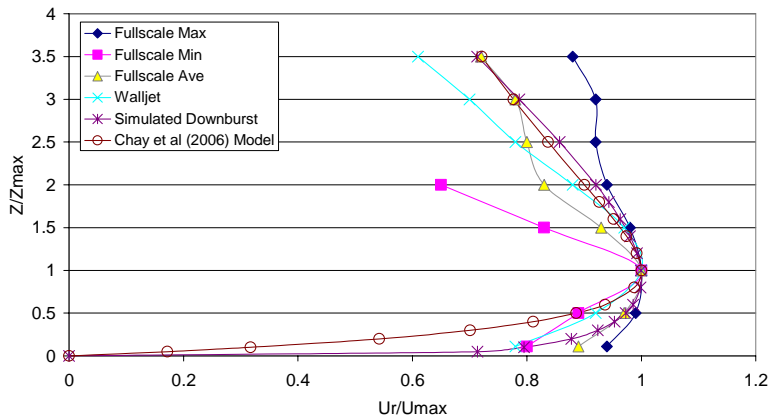


Figure 1: Comparison of simulated non-turbulent downburst winds with full-scale observations

The model is an improvement of the one described in Chay et al (2006). The primary difference is a change to the shape of the radial distribution as a function of height. The shape of the profile has been changed, and is based on the profile described by Wood et al (2001) in order to provide better agreement with near ground full-scale observations (Hjelmfelt, 1988) (Figure 1). Recent numerical and physical modelling (Mason et al, 2005; Kim et al, 2005) suggest that the profile may in fact be flatter over much of the elevation at which the fastest wind speeds occur, which could potentially lead to more onerous loads than those predicted by the current model. However, these simulations are yet to be verified against full-scale data, which is in very short supply. The shortage of full-scale downburst data remains a major stumbling block for research relating to the affects of downbursts on structures.

The model draws on the best features of other methods, the selection of which is discussed in Chay et al (2006). The main advantage of this method over other simple analytical, numerical or empirical models is inclusion of a time intensity factor that can include the initial period of intensification at the start of an event as well as it's decay in strength after it's peak, and a radius to maximum wind speed that is also a function of time to model the expansion of the wind field as it ages. It also allows the user to adopt a height of maximum wind speed that is radially dependent. While it may not allow for as close a recreation of specific events as some more recently published methods (eg Chen and Letchford, 2005), the more generalised parametric approach adopted here allows the user greater control of the physical characteristics of the downbursts they wish to investigate.

Readers should note that the model uses a moving reference frame. That is to say that the centre of the storm ($r=0$) moves with respect to stationary objects on the ground. The storm moves at the same speed and in the same direction as \bar{U}_{Trans} . When using this method, users should consider a range of proximities of there structure to the centre of the storm.

Figure 2 displays a relative comparison of the design code profile and the simulated downburst horizontal wind speed profile, in which all speeds are normalised by the mean speed at 10m AGL. Terrain category II is assumed for the boundary layer wind (open grasslands). The simulated downburst has an assumed height to maximum wind speed of $z_m = 100\text{m}$, and a translational speed of $\bar{U}_{Trans} = 0\text{m/s}$. Note that these are not design gust profiles, which vary slightly due to the relationship between the turbulence and mean speed. This is discussed later in section 3.0.

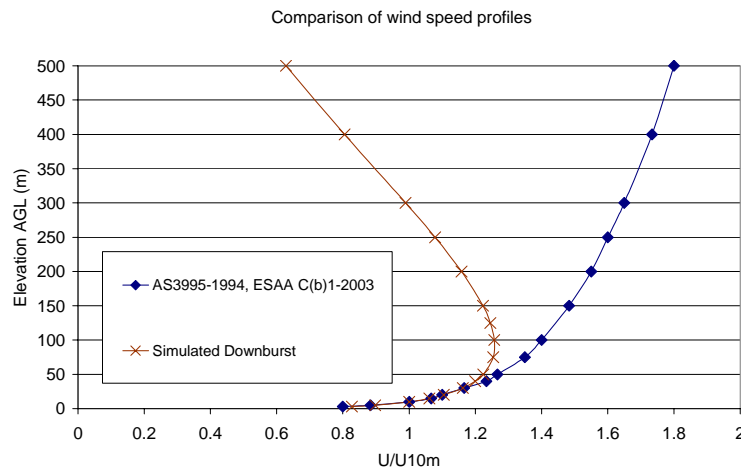


Figure 2: Comparison of simulated downburst non-turbulent winds with standardised boundary layer mean speed winds.

The simulated downburst winds have a vertical component, the magnitude and direction of which is a function of proximity to the downburst centre. Figure 3 shows the vertical component of a simulated downburst at a variety of radial distances from the centre of the storm. The wind speeds are normalised with respect to the horizontal non-turbulent wind speed 10m AGL at r_p , and the elevations normalised with respect to the height at which the maximum non-turbulent horizontal wind speed occurs. All profiles are for open grasslands. Note that for simplicity, the simulated downburst has an assumed height to maximum wind speed that is constant with varying radius ($z_r = z_m = 100\text{m}$), and a translational speed of $\bar{U}_{Trans} = 0\text{m/s}$. The downburst does not vary in size or strength with time ($\Pi = 1$, $r_r = r_p$), and the radius to maximum wind speed is assumed to be 1500m, which is also the radius at which the profile is plotted in Figure 2.

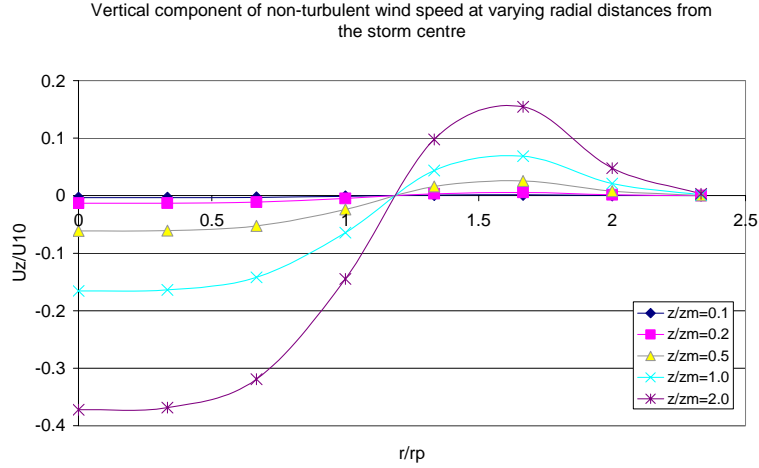


Figure 3: Vertical component of the simulated non-turbulent downburst winds.

Close to the centre of the downburst, there is a significant downward (negative) component to the wind, which reduces in strength to a point slightly beyond r_p . There is a region of positive wind speeds beyond this point, and at large radial distances the wind speed is 0.

This is contrary to boundary layer winds, which are assumed to have no mean wind speed component in the vertical direction. As Figure 3 indicates, the vertical component of the vertical wind speed in the simulated downburst is significant from a structural loading perspective, and warrants further attention.

2.3 Wind Speed Footprint

Whereas a boundary layer wind can be thought of as having a constant mean speed at a given height over large areas and for long periods of time, the simulated downburst wind field is highly localised and shows variation in intensity with varying proximity to the storm and with varying event duration. Consider a simulated downburst with a translation speed of $\bar{U}_{Trans}=10\text{m/s}$ and maximum non-turbulent radial speed of $\bar{U}_{r,max}=40\text{m/s}$ (giving an anticipated largest value of \bar{U}_r of 50m/s). The radius to maximum wind speed of the storm is expanding at 125m/min , $r_p=1375\text{m}$, and has a linearly varying intensity factor of

$$\Pi = \begin{cases} t/5 & \text{for } t \leq 5 \text{ min} \\ \frac{1-(t-5)}{8} & \text{for } 5 < t \leq 13 \text{ min} \end{cases} \quad (5)$$

Where t is time in minutes from the start of the event.

A record of the largest wind speed occurring during the passage of the event was kept at a number of points in the horizontal plane (at a height corresponding to the height of the maximum horizontal wind speed, which in this particular case is arbitrary). In this case only the horizontal component of the non-turbulent winds was considered, and wind speeds were normalised by 50m/s , the largest possible wind speed. Figure 4 shows a contour plot of this 'footprint'.

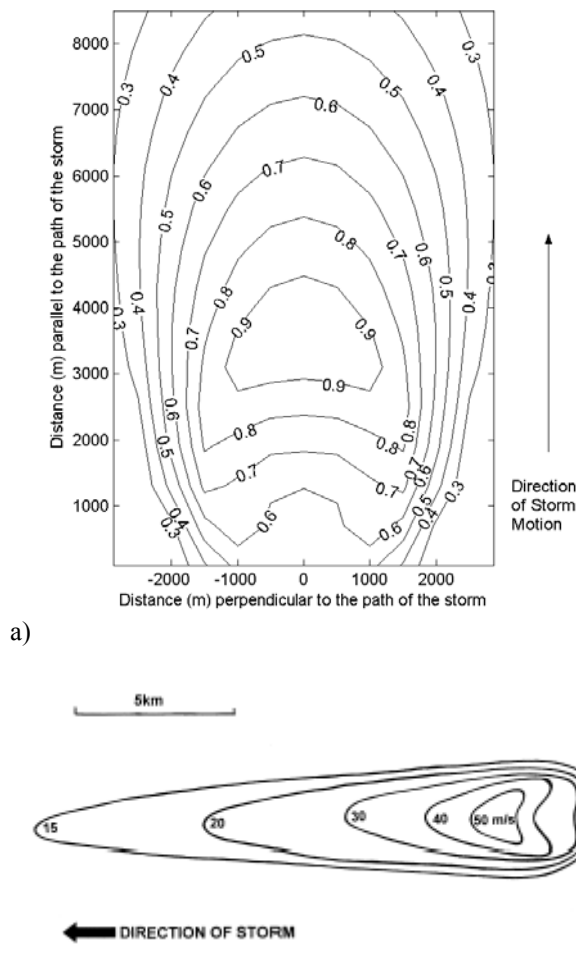


Figure 4: Wind speed footprints generated by a) the simulated downburst described by equation (3) and b) Holmes and Oliver (2000).

The image is very similar to the footprint published by Holmes and Oliver (2000), although shows a widening of each contour area at the forward half of the footprint that was not present in the Holmes and Oliver case. This widening is due to the expansion of the simulated downburst in the present study. The Holmes and Oliver footprint is significantly longer due variation in the decay rate of the storm (linear in simple example provided versus the exponential decay in the Holmes and Oliver Model).

Wind directionality is also important to consider, as due to the radially diverging nature of a downburst flow, wind vectors in an event are not parallel in all regions of the storm. A vector plot of the footprint shown above is shown in Figure 5. The largest wind speeds during the event occur at the along the central axis of motion of the storm (0m on the x-axis of Figure 5) and are in the direction of storm motion. This is due to the vector addition of translational velocity of the storm radially diverging winds, a technique which has been adopted in many cases in the literature (eg Letchford and Mans, 2000; Holmes and Oliver, 2000; Letchford and Chay, 2002; Chay et al, 2006). However, the further the point of observation moves away from the central axis of the storm (0m on the x axis), the higher the angle between the direction of the storms motion and the direction of the highest wind at that point. This is contrary to the nature of a boundary layer wind, which is conceptualised as flowing in the same direction over large areas, and has particular significance when considering consecutive towers in a transmission network.

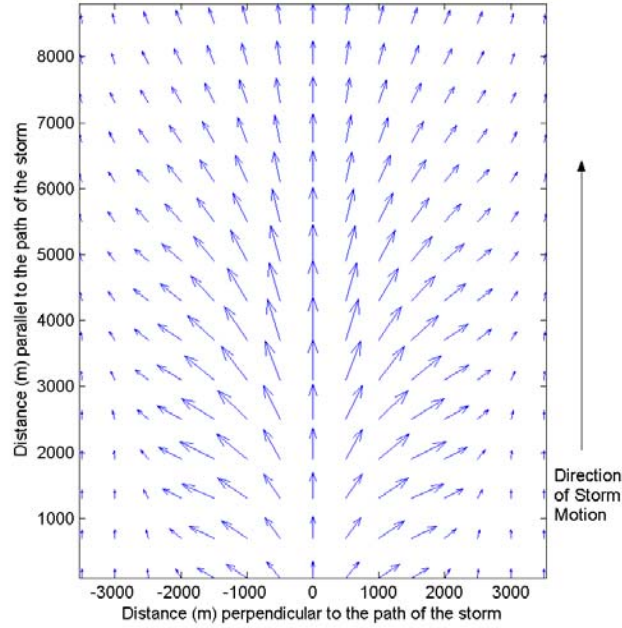


Figure 5: A vector plot of the wind speed footprint created by the simulated downburst in Equation (3).

3.0 GUST FACTORS

The different design codes treat the relationship between the mean profile and gust profile in a variety of ways. AS3995-1994 and ESAA-C(b)1-2003 relate the mean speed to the design gust speed with the equation:

$$V = V_m \left(1 + 3.7 \left(\frac{\sigma_v}{V_m} \right) \right) \quad (6)$$

Where V_m is the hourly mean speed and σ_v is the standard deviation of the wind gust component. The value 3.7 is based on a probabilistic approach to what intensity gust can be reasonably expected to occur during a given period. Alternatively, the shape of the profile is tabulated.

Due to the short term nature of downburst winds, gusts that are extremely large in relation to the non-turbulent component of the wind are less likely to occur. However, there is much difficulty associated in trying to estimate the likelihood of a fluctuation of certain strength in a non-stationary stochastic process that has been superimposed on a non-stationary base process. To help quantify a suitable value for relating value to relate gust and ‘mean’ speed, a series of tests were performed in which sine waves of varying period were used to simulate the non-turbulent winds of downbursts are a variety of sizes and durations.

Fine scale fluctuations are imposed on the non-turbulent winds to simulate the turbulence occurring during a downburst. These fluctuations are created using an ARMA process, and when used with a suitable spectral density function and coherence functions, can be used to generate simultaneous turbulence time histories at multiple points in space and in multiple directions (x, y and z). Samaras et al (1984) describe a suitable ARMA method. When used in the manner summarised in Chay et al (2006), the output of the ARMA method is a Gaussian time history with a mean of 0 and a variance of 1. The time history is then amplitude modulated in proportion to the non-turbulent wind speed at the at which any given fluctuation is occurring.

$$U(t) = \bar{U}(t) + u'(t) \quad (7)$$

and

$$u'(t) = I_u \bar{U}(t) \Psi(t) \quad (8)$$

where $\Psi(t)$ is the Gaussian time history, and I_u is the desired turbulence intensity.

There is much uncertainty regarding the turbulence intensities occurring during downbursts, largely due to the overwhelming lack of full-scale observations that are suitable for characterising this property. Physical and numerical simulations (Chay, 2001; Kim et al 2005) suggest that over the height of a tall structure the turbulence may be relative uniform at the location of maximum wind speed. However, recent full-scale observations (Chen and Letchford, 2005) at low levels above the ground suggest that there is variation in intensity with varying height. Chen and Letchford observed turbulence intensities over several points with 15m AGL, and suggested:

$$I_u(z) = I_{u10} \left(\frac{10}{z} \right)^{1/6} \quad (9)$$

where I_{u10} is in the order of 0.088. This results in turbulence intensities in the order of 5% to 10% over the height of a tall structure. As such, tests were performed assuming a turbulence intensity of 5%. Sine wave period (T) ranged between 50 seconds and 2500 seconds, and turbulence was generated at a variety of time intervals (δt) ranging between 0.2 seconds (5Hz) and 3 seconds (0.33Hz). Although there is very recent evidence to suggest that the spectral density function of downburst turbulence is different to that of boundary layer turbulence, a simplifying assumption has been made that the Kaimal Spectrum (Kaimal et al 1974) is applicable. As a rough approximation, the sine wave can be related to the storm conditions for a point that is directly traversed by the storm through the relationship:

$$T = \frac{4r_t}{U_{Trans}} \quad (10)$$

To bring this into perspective, a storm moving at 10m/s with a radius to maximum speed of 1500m has a period of approximately 600 seconds. 200 storms were generated for each set of conditions. In order to compare the peak wind speed to the peak non-turbulent wind speed, the maximum gust from each storm was expressed as a Gust Factor (GF), which is the number of standard deviations above the maximum non-turbulent speed:

$$GF = \frac{U_{MAX} - \bar{U}_{MAX}}{I_u \bar{U}_{MAX}} \quad (11)$$

The GF values from each set of tests were ranked, and an empirical relationship was determined for the 50th, 75th and 95th percentile as a function of sine period:

50th percentile:

$$GF = 0.4 \ln \left(\frac{T}{\delta t} \right) - 0.75 \quad (12)$$

75th percentile:

$$GF = 0.4 \ln \left(\frac{T}{\delta t} \right) - 0.4 \quad (13)$$

95th percentile:

$$GF = 0.3 \ln \left(\frac{T}{\delta t} \right) + 0.9 \quad (14)$$

Therefore, for the storm with a period of 600 seconds, a gust factor for a 3 second gust at the 95th percentile would be in the order of 2.5. Tests involving stationary processes indicate that this has approximately the same likelihood of a achieving a gust 3.7 standard deviations above the mean for a one hour statistically stationary wind using 0.33Hz turbulence.

For uniform turbulence, this does not change the shape of the gust profile for the simulated downburst, which under these conditions will be the same shape as the non-turbulent wind speed. Three design gust profiles are shown in figure 6. The first is the shape of the gust profile tabulated in AS3995-1994. The second is the design gust profile of the simulated downburst, assuming turbulence intensity is uniform with height. The third profile is the simulated downburst assuming the Chen and Letchford turbulence intensity profile. The downbursts are assumed to have peak speeds at 100m

AGL, and 0 translational speed. All speeds have been normalised with respect to the speed at 10m AGL.

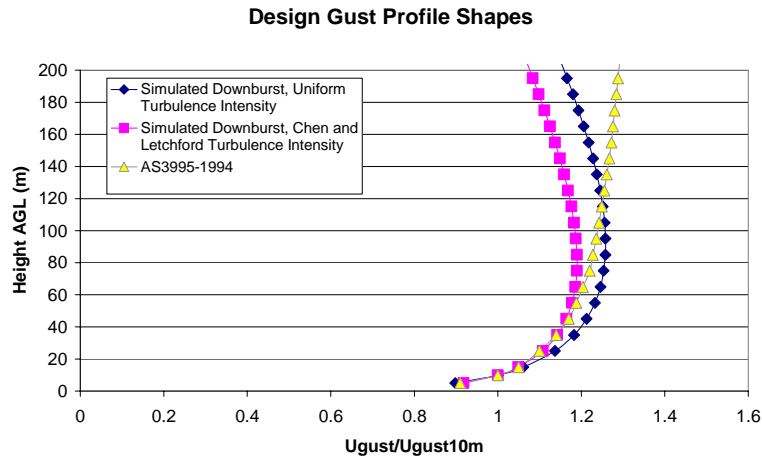


Figure 6: Comparison of design gust profiles for the simulated downburst with varying turbulence intensity profiles and AS3995-1994

For the same 10m gust speed, the uniform turbulence intensity profile greatly exceeds the boundary layer profile for heights less than 120m. The Chen and Letchford (CL) turbulence intensity case slightly exceeds the boundary layer profile for heights under 60m, however is sensitive to the GF value used. For lower GF's, the CL case exceeds the boundary layer profile by great amounts, and vice versa. At higher GF's, the CL winds are weaker than the boundary layer profile about the 10m level.

However, there is a good deal of sensitivity between the assumed parameters of the simulated downburst and the design pressures the model generates. Simulated downbursts with a variety of assumed translational speeds and heights to maximum wind speed are shown below in figure 7. For all downbursts shown below turbulence intensity was assumed to be uniform, and the 10m speed to be 60m/s. The design pressure is simply $\frac{1}{2}\rho U^2$.

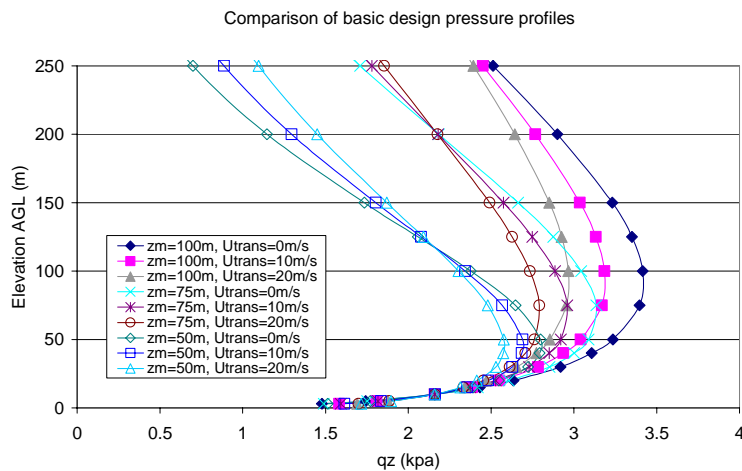


Figure 7: Sensitivity analysis of downburst design pressure profile parameters

The spread of the profiles demonstrates the high sensitivity to certain parameters. It also emphasises the need to accurately characterise the typical dimensions of downbursts in particular areas. Obviously it is necessary to design for the worst conditions in an area. However, assuming the worst possible parameters without accurate knowledge of the scale of events occurring in an area could lead to designs that are extremely conservative, resulting in unnecessary expense due to overly heavy construction.

4.0 SPAN REDUCTION FACTORS

The difference between the gust speed and mean speed is smaller than currently predicted using AS3995-1994 or ESAA C(b)1-2003. The variation in gust factor is also quite relevant to dynamic design and also to load reduction factors which assume certain degrees of correlation between wind speeds over large areas, and in particular, the load along long span conductors. ESAA C(b)1-2003 specifically address the subject of load reduction factors on long span conductors. For terrain category 2, in regions A and B, the Span Reduction Factor (SRF) is given by:

$$SRF = 0.58 + 0.42e^{\left(\frac{-L}{180}\right)} \quad (15)$$

Where L is the span in metres. However, it goes on to state that: “*The span reduction factors used to calculate conductor wind forces for synoptic winds are not representative of the horizontal velocity profiles for microbursts. Experimental data and tower failure investigations indicate that an appropriate span reduction factor is in the order of 0.9*”

This approximate value is relatively coarse compared to the precise nature of many other factors in the design process.

An investigation was performed, in which 10 storms were simulated. For simplicity, the values of $\Pi=1$ and $r_t=1500\text{m}$ for all values of t were used. Wind speeds were generated at 2.5m intervals along a 400m span perpendicular to the direction in which the storm was moving, and a height of $z=25\text{m}$ ($z_m=z_r=100\text{m}$). The span was centrally located with respect to the storm's line of motion. Turbulence was generated 5Hz, and was assumed to be 5% or 10%. The wind speed time histories were converted to pressures, and the pressures were averaged along the span for various lengths ranging between 20m and 400m (all central to the storm's line of motion) for each time step. Only the component of the wind perpendicular to the span was considered. For each storm, the span reduction factor was defined as that largest value of the average load across a given span length ($F_{MAX.AVE.L}$) divided by the largest instantaneous value of loading occurring anywhere within the 400m span ($F_{MAX.POINT.400m}$).

$$SRF = \frac{F_{MAX.AVE.L}}{F_{MAX.POINT.400m}} \quad (16)$$

Results are shown in comparison to the ESAA values in Figure 8. An average of the SRF values for the 10 storms is shown, and also the largest value from the 10 storms for each length is shown. For spans of greater than 150m, the simulated downburst with 5% turbulence produces Span Reduction Factors that lie between the two predictors provided in ESAA C(b)1-2003. However, the reason for the differences lies primarily with the turbulence intensity and short term nature of the storm. Due to the lower turbulence and brief duration the wind gusts occurring in a downburst along a span show less variation from the non-turbulent speed than during boundary layer flow, meaning that loading is likely to be more similar over all points of the conductor during the downburst. The SRF values for the 10% turbulence storms were lower than the two ESAA predictions. However, it would appear that at larger spans (>500m) the downburst SRF for 10% turbulence would intersect or exceed the boundary layer prediction. It should be noted that, from the observations by Chen and Letchford (2005), 10% turbulence appears to be very high for downburst wind conditions. In both cases, the reduction factors from the simulated downbursts are substantially lower than the ESAA estimate of 0.9. The values in the above figure are somewhat lower than the long span loading shown in Holmes and Oliver (2000). However, the Holmes and Oliver example appears to exclude the effects of fine scale turbulent fluctuations, which leads to an overestimate of the correlation of the load.

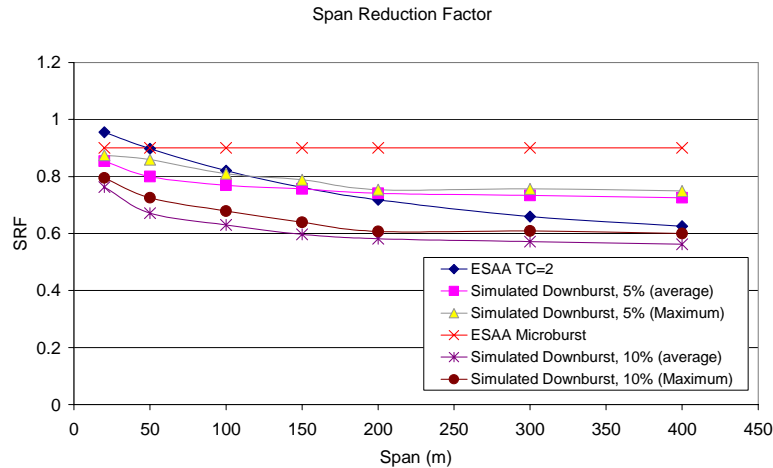


Figure 8: Comparison of Span Reduction Factors

Changes in the physical size of the storm would result in changes in the profile, although over the range of downburst sizes that can be reasonably expected, these differences would be relatively minor. Varying the turbulence intensity would have a more substantial affect. Increasing the turbulence intensity would result in a reduction of the SRF, as the wind gusts along the conductor become more erratic.

5.0 AN EXAMPLE OF LOADING ON A THEORETICAL TOWER

A simple theoretical tower was considered as an example for examining the relative levels of loading prescribed by the different design codes. The tower has the following properties:

- A height of 50m
- A constant width of 3m
- A constant solidity of 0.2138 for one face or 0.2609 total projected area.
- Two conductors, both with a diameter of 45mm and spanning 300m, attach to the tower at a height of 45m. For simplicity, the conductor is assumed to be 45m AGL for its entire length.

In practical terms, the tower is somewhat unrealistic, although is useful for demonstrating differences between loading philosophies as it is simple and its properties are consistent.

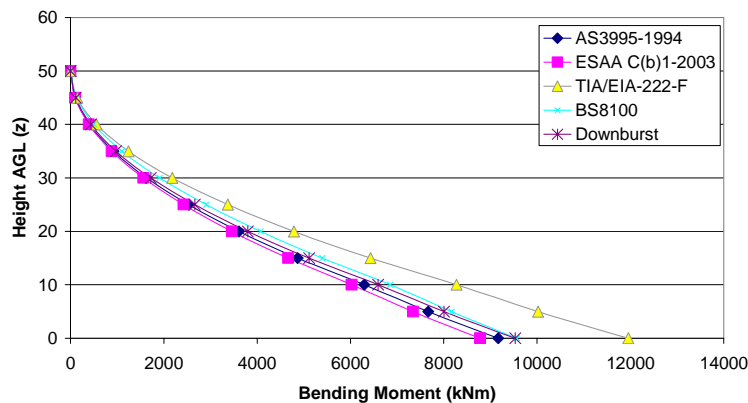
The various codes under consideration give basic wind speeds for determining loads that are particular to their region. As we are trying to assess the various codes of practice relate to one particular tower, the basic wind speed has been selected from ESAA C(b)1-2003. TIA/EIA-222-F, ESAA and AS3995 all use gust speeds as their basic wind speed, and so the 1000-year return period in ESAA Region II (70.8m/s), which is a specific to downburst activity in South-East Queensland, was used for these standards. Note that adopting the basic wind speeds from the other codes, including AS3995-1994 which specifically deals with South-East Queensland) would lead to substantially lower loads, as the wind speeds listed are well below the ESAA values. In fact, had the AS3995 loads been based on the AS3995 basic wind speed, the loads for this standard would have been in the order of 55% lower. BS8100 is based on a 50-year return period hourly mean speed. Although this has no mean for a downburst, a relation ship in Appendix A of that standard was used to reduce the basic wind speed to an appropriate value. This was applied to the 50-year return period gust speed (56.0m/s) in ESAA.

Bending Moments and Shear Forces were calculated for the tower for each code under the assumption that the tower was divided into 10 segments, which design pressure being determined at mid height of each segment. The simulated downburst profile was also investigated in comparison to the codified wind descriptions. The storm was assumed to have the parameters $r_i=r=1500m$, $z_r=z_m=100m$, $\bar{U}_{Trans}=0m/s$, $\bar{U}_{Trans}=89.1m/s$ (which results in a wind speed of 70.8m/s at 10m AGL, and ESAA tower drag coefficients. For simplicity, the vertical component of the wind has been ignored, although this would certainly affect the loading in the tower. The turbulence intensity of the downburst has been assumed to be 5%, and uniform with height.

Figure 9 shows the bending moments and shear forces on the tower as per the various design codes. The TIA moments and shears were substantially larger than the other loading methods considered. This is possibly due to the use of a gust factor, which is used to elevate the loads caused by a low basic wind speed (50 return period), which is possibly not applicable in this case. This is an

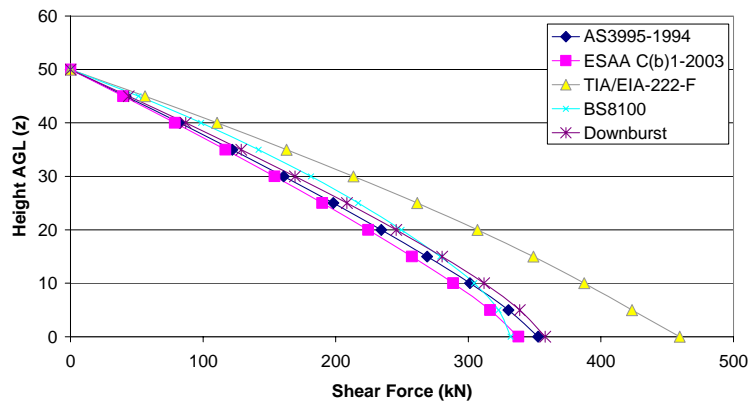
unfortunate difference in the manner in which the wind loading assessment process is dealt with, and the authors were unable to determine a more suitable method of comparing the TIA standard with other codes. When the ESAA 50-year return period wind was used, the TIA loads were substantially lower than the Australian codes, which only proved that the gust factor did not elevate the 50-year wind to a 1000-year wind. In a subsequent analysis using the 1000-year return period wind, this gust factor was excluded, and the resulting moment and shear distributions were almost identical to the simulated downburst case. BS8100 produced bending moments that were slightly higher than the Australian standard estimates and the simulated downburst, which is likely a result of the variation between the models for the boundary layer profile (BS8100 uses the power law, while the Australian codes adopt the Deaves and Harris model (Standards Australia, 2002b)). The shear force estimated by BS8100 was slightly lower at the base of the tower than the other codes, despite being larger over much of the tower's height. This is likely caused by an assumption regarding the distribution of force in the bracing, which affects a component of the BS8100 shear gust factor, due to the absence of a detailed truss analysis.

Comparison of Tower Bending Moments



a)

Comparison of Tower Shear Forces



b)

Figure 9: Bending Moment and Shear Force diagrams for the theoretical tower.

It is interesting to note that the downburst wind loads exceeded both ESAA (8.5% BM and 6.2% SF at the tower base) and AS3995 (3.1% BM and 1.6% SF at the tower base), despite being modelled on the ESAA drag coefficient, which was lower than that in AS3995. From Figure 6, in which it was demonstrated that the downburst wind speeds were higher than the boundary layer cases to a height of approximately 110m AGL for the assumed downburst parameters, it can be inferred that the difference would be greater for a tower of approximately this height. Conversely, in situations when towers are significantly higher than 110m, the loading on towers can be significantly lower in downbursts than in boundary layer winds, for a given 10m gust speed, and current practices may be leading to excessively strong designs.

Table 1: Comparison of conductor loads for the theoretical tower

Standard	Qz (kPa)	Cd	SRF	Force per Conductor(kN)	Base Bending Moment (kNm)	Total Shear (kN)
AS3995-1994	4.01	1.2	1	65.0	5851.5	130.0
ESAA C(b)1-2003	4.01	1	0.9	48.8	4388.6	97.5
TIA/EAI-222-F	4.72	1.2	1	95.6	8606.5	191.3
BS8100	2.15	0.9	0.75	41.4	3726.1	82.8
Downburst	4.43	1	0.756	45.2	4067.4	90.4

Table 1 shows the additional shear force and base bending moments caused by the conductor loading, as predicted by the various codes. Note that AS3995 and TIA do not specifically address conductors, and as such, do not make provision for span reduction. The conductors were dealt with as linear ancillaries in these cases. Again, TIA estimated the highest loads, due to the highest design pressures and the highest drag coefficient, and the gust factor. However, despite having a higher design pressure than the two Australian standards, the simulated downburst resulted in lower conductor loads than ESAA or AS3995. This is primarily due to the Span Reduction Factor. In this particular case, the ESAA downburst factor was used (0.9), which was significantly higher than the 0.756 (max. value for 5% turbulence as predicted in Figure 68. Had the boundary layer value of the SRF been used, the downburst wind loads would have been substantially higher than the ESAA case. The BS8100 conductor loads were the lower than the downburst case despite similar SRF values. This is partially due to the inclusion of a cable height factor in the British code, which results in a further load reduction in this case.

6.0 CONCLUSIONS

The results presented highlight clear differences between the way in which wind is presented in design standards and the loading scenarios produced by the simulated downburst. Aside from the large differences in basic wind speeds between boundary layer and downburst winds, the downburst load simulations indicate that:

- Loads on lattice towers in downbursts may currently be underestimated by a significant amount due to variations in the distribution in wind speed with height, and also due to a vertical component to the wind that is not a feature of boundary layer winds
- For a given gust speed, wind loads on long span conductors (greater than approximately 150m) are likely to be higher in downbursts than in the ESAA estimate for boundary layer winds, although lower than estimated by ESAA for downbursts.

This variation means that there is likely to be a degree of error in any structural or risk assessment efforts of transmission line structures in thunderstorm prone areas that are based on boundary layer wind loads.

Unfortunately, the study also highlights the sensitivity of loading estimates certain downburst parameters. It would seem that until there is a concerted effort to accurately observe and record the scale and intensity of downburst events occurring in specific regions, this uncertainty will remain an inherent characteristic of downburst loading estimates, meaning that they can largely only be regarded as preliminary.

7.0 ACKNOWLEDGEMENTS

The authors would like to thank Dr. Richard Wilson for his assistance with this project, and *Powerlink QLD* for their financial support.

7.0 REFERENCES

British Standards Institute (1986). "BS8100:Part 1:1986 Lattice Towers and Masts Part 1. Code of practice for loading." *British Standards Institute, London, UK*, 66 pages.

Chay, M. T. (2001). "Physical Modeling of Thunderstorm Downbursts for Wind Engineering Applications," MSCE, Texas Tech University, Lubbock, TX USA.

Chay, M. T., Albermani, F. and Wilson, R. (2006). "Numerical and analytical simulation of downbursts for investigating dynamic response of structures in the time domain". *Engineering Structures*, 28, 240-254.

Chen, L. and Letchford, C.W. (2005) "Simulation of Extreme Winds from Thunderstorm Downbursts" *Proceedings of the Tenth Americas Conference on Wind Engineering*, May 31-June 4 2005, Baton Rouge, Louisiana, USA.

Electrical Supply Association of Australia (2003) "ESAA C(b)1-2003 Guidelines for design and maintenance of overhead distribution and transmission lines" *Standards Australia, Sydney, Australia*, 164 pages.

Holmes, J. D., and Oliver, S. E. (2000). "An empirical model of a downburst." *Engineering Structures*, 22, 1167-1172.

Kaimal, J.C., Wyngaard, J.C., Izumi, Y. and Cote, O.R. (1972). "Spectral Characteristics of surface-layer turbulence". *Quarterly Journal of the Royal Meteorological Society* Vol. 98, 563-589.

Kim, J., Ho, T.C.E and Hangan, H. (2005). "Downburst induced dynamic responses of a tall building." *Proceedings of the Tenth Americas Conference on Wind Engineering*, May 31-June 4 2005, Baton Rouge, Louisiana, USA.

Letchford, C.W. and Mans, C. (2000). "Translation effects in modeling thunderstorm downbursts." *Fourth International Colloquium on Bluff Body Aerodynamics and Applications*, 11-14 September 2000, Bochum, Germany, 175-178.

Mason, M.S., Letchford, C.W., and James, D.L. (2005). "Pulsed wall jet simulation of a stationary thunderstorm downburst, Part A: Physical structure and flow field characterization." *Journal of Wind Engineering and Industrial Aerodynamics*, 93, 557-580.

Standards Australia, (1994) "AS3995-1994 Design of steel lattice towers and masts" *Last accessed online on 1 November, 2004*, 64 pages.

Standards Australia, (2002a) "AS/NZS 1170.2-2002 Structural design actions Part 2: Wind Actions" *Accessed online on 11 January, 2006*, 88 pages.

Standards Australia, (2002b) "AS/NZS 1170.2 Supp 1:2003 Structural design actions-Wind Actions-Commentary (Supplement to AS/NZS 1170.2:2002)" *Accessed online on 11 January, 2006*, 56 pages.

Telecommunications Industry Association (1996) "TIA/EIA-222-F Structural Standards for Steel Antenna Towers and Antenna Supporting Structures" *Telecommunications Industry Associations, Arlington, VA, USA, reproduced by Global Engineering Documents*, 115 pages.

Wood, G. S., Kwok, K. C. S., Motteram, N. A., and Fletcher, D. F. (2001). "Physical and numerical modelling of thunderstorm downbursts." *Journal of Wind Engineering and Industrial Aerodynamics*, 89, 532-552.